J Mater Sci (2022) 57:5384–5395

Chemical routes to materials

Preparation and characterization of high-performance Ni-based core–shell catalyst for ethanol steam reforming

Tamara S. Moraes[1,*], Vanderlei S. Bergamaschi[1], João C. Ferreira[1], and Estevam V. Spinacé[1]

[1] *Instituto de Pesquisas Energéticas e Nucleares, IPEN/CNEN, Av. Prof. Lineu Prestes, 2242-Cidade Universitária, São Paulo, SP 05508-000, Brazil*

Received: 27 October 2021
Accepted: 24 January 2022
Published online: 21 February 2022

ABSTRACT

A core–shell catalyst, based on nickel nanoparticles supported on silica nanospheres and surrounded by ceria, was tested for ethanol steam reforming (ESR) reaction (H_2O/ethanol: 3/1) under low-temperature conditions (400, 500 and 600 °C) in order to test its stability during the reaction. Two other catalysts of Ni supported in SiO_2 and CeO_2 were also synthesized to be compared with the core–shell catalyst in the ESR. All catalysts showed excellent activity at 500 and 600 °C with 100% ethanol conversion. Increasing the reaction temperature, carbon deposition on the surface of the catalysts decreases throughout the reaction. The core–shell catalyst showed high coke inhibition capacity in the ESR at 600 °C, without coke formation for at least 100 h of reaction. On the other hand, after 20 h of ESR at 600 °C, Ni–SiO_2 and Ni/CeO_2 catalysts showed formation of 6.3 and 5.2 mgC/(gcat.h) of coke, respectively. The strong redox capacity of ceria together with the change in catalyst structure due to the deposition of cerium oxide on top of Ni particles led to an excellent ESR activity of this catalyst.

Introduction

Currently, the world dependence on technologies that provide energy sources originate from fossil fuels (coal, oil products and natural gas), the management of residues resulting from anthropogenic activities and the mitigation of environmental impacts, such as the production of polluting gases and the global warming, are three problems that humanity is facing. In order to minimize these problems, there has recently been an intensification in the search of alternatives for energy production, in particular by the use of biofuels.

Handling Editor: Catalin Croitoru.

Address correspondence to E-mail: tamara.moraes@ipen.br

https://doi.org/10.1007/s10853-022-06969-4

Ethanol derived from biomass (bioethanol) is an important renewable resource [1]. Several technologies can be used to obtain a hydrogen-rich stream from ethanol, such as steam reforming, partial oxidation and oxidative reforming of ethanol [2]. Some of the advantages of using ethanol as an energy source is the low toxicity compared to gasoline and methanol, and also the fact that countries like Brazil and the US already have the necessary infrastructure for its production and distribution.

Among the catalysts studied for the ESR reaction, nickel-based catalysts showed the highest activity and selectivity in terms of H_2, in addition to being low cost compared to noble metals [3–5]. However, the commercialization of this technology finds some obstacles like the deactivation of the catalysts due to carbon formation [6–9]. So, it is necessary to search for catalysts that are stable and avoid carbon formation under steam reforming conditions.

Cerium oxide has the ability to remain structurally stable even with a significant loss of oxygen, leading to the formation of a large number of vacancies in its structure [10–12]. The high oxygen storage and oxygen mobility capacity present in the CeO_2 structure can contribute to avoid catalyst deactivation by removing carbon from the surface of the catalyst [13–15].

Another approach to minimize coke formation is to control the size of the metallic particles through modifications in the catalyst structure. According to the mechanism reported in literature, carbon formation in these reactions is favored by large metal particles [16]. Therefore, controlling particle size, and its sintering process, is essential to reduce the accumulation of carbon on the catalyst's surface during ethanol reforming reactions [16].

One strategy for inhibiting the sintering process of metal particles in catalysts is the development of core–shell catalysts [17]. Such catalysts feature a metal core covered with an oxide layer, which accelerates the conversion processes of the carbon formed at the metal-oxide interface, favoring the gasification reaction and consequently its elimination in the form of CO_2. Das et al. [18] have synthesized a core–shell structured catalyst based on Ni and CeO_2 exhibiting a high performance at dry reforming of biogas, with negligible coke formation. They also synthesized Ni–SiO_2 catalyst, which showed extensive coke formation and low activity. The higher activity of the core–shell catalyst was attributed, by the authors, to the higher dispersion of Ni on the catalyst's surface. The high efficiency of this catalyst in inhibiting coke deposition in the dry reforming of biogas suggests that this catalyst could also be efficient in ethanol steam reforming reactions.

The aim of this work is to evaluate the performance of the structurally modified Ni–SiO_2@CeO_2 catalyst in the form of core–shell based on nickel (Ni–CS) in the inhibition of carbon formation and in the increase of the catalyst's stability in the ERS reaction. This new form of catalyst synthesis has proved to be very efficient in other reactions, but it has not been studied in the ESR reaction yet.

Experimental

Synthesis of catalysts

The structurally modified catalyst in the form of core–shell Ni–SiO_2@CeO_2 (Ni–CS) and Ni–SiO_2 catalysts were prepared using the route previously described by Das et al. [18] (Fig. 1). First, SiO_2 nanospheres were synthesized by Stöber method [19–21] and then Ni was deposited on them by wet impregnation using a nickel nitrate solution as a precursor. Catalysts were prepared with 10 wt% Ni. The sample was calcined to prepare the Ni–SiO_2 catalyst. Ni–CS was prepared by precipitation using the Ni–SiO_2 sample before calcination and cerium nitrate as the precursor. Figure 1 shows the synthesis route for Ni–SiO_2 and Ni–CS catalysts.

For Ni/CeO_2 catalysts synthesis containing 10 wt% of Ni, first, the CeO_2 support was prepared by precipitation method using $Ce(NO_3)_3{\cdot}6H_2O$ as the precursor and NaOH solution as the precipitant. After precipitation, the solid was washed with water and dried at 100 °C. Then, the precipitate was calcined at 500 °C for 5 h. The support was impregnated by incipient wetness impregnation with an adequate amount of nickel using nitrate hexahydrate as a precursor. The sample was dried (100 °C) during 12 h and then calcined (400 °C) for 4 h.

Catalyst characterization

The specific BET area, pore size and pore volume of the materials were measured by the ASAP 2020 equipment from micromeritics. The analysis was carried out through the physical adsorption of

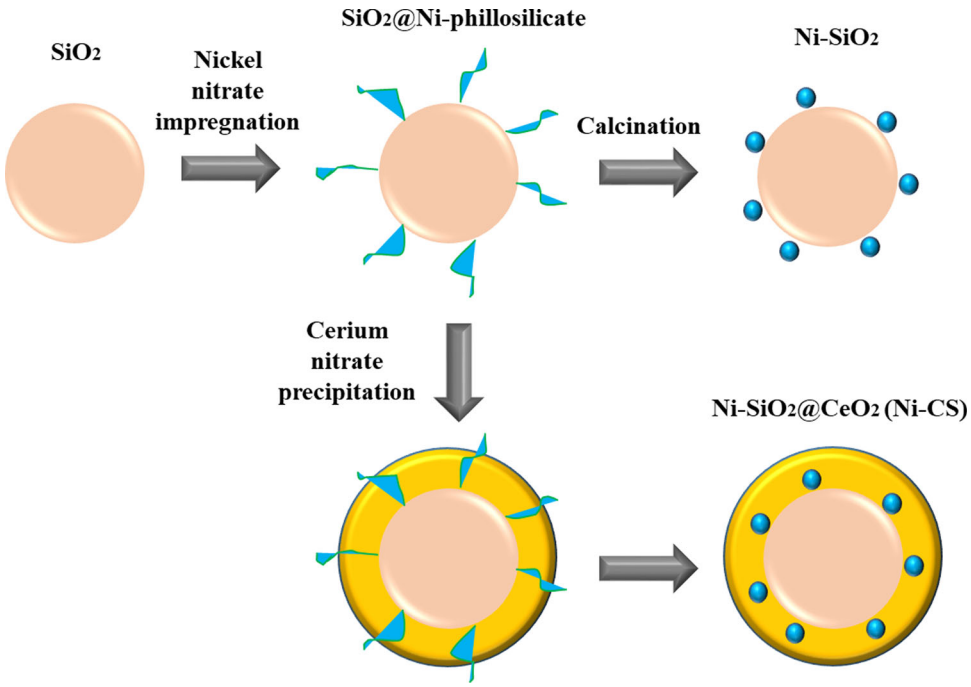

Figure 1 Synthesis route for Ni–SiO_2 and Ni–CS catalysts. (Adapted from Das et al. [18]).

nitrogen at − 196 °C, using 200 mg of catalyst. The sample underwent a pre-treatment in situ, which consisted of heating the sample at 350 °C until reaching a vacuum of 9 µm Hg. Then, the sample was weighed to obtain its real mass. The pore size was calculated using the BET method, and the pore volume was calculated using the BJH method.

The chemical composition was determined in a semi-quantitative way by energy-dispersive X-ray spectroscopy (EDX) in a Shimadzu EDX-700 equipment, with a Rh X-ray tube.

Crystallographic information of the catalysts was analyzed by X-ray diffraction (XRD) in the Rigaku diffractometer model Miniflex II equipped with Cu Kα radiation source. The X-ray diffraction patterns were recorded with a step size of 0.05° at different 2θ (20° to 90°).

Temperature-programmed reduction analysis (TPR) was used to verify the behavior of the catalysts in the presence of a H_2-reducing atmosphere in QuantaChrome Chem BET/TPR. The morphologies of the catalysts were examined by a transmission electron microscope (TEM-FEG JEM-2100F, 200 kV).

In-situ DRIFTS analyses were performed on a Bruker VERTEX 70 spectrometer. The analyses were performed with a resolution of 4/cm, and 256 scans were accumulated in order to improve the signal/noise ratio. The detector used for these analyzes was the liquid nitrogen detector (LN-MCT). Before adding catalysts to the IV and starting the DRIFTS analysis, all catalysts were previously reduced under H_2 flow (30 mL/min) at 800 °C for 2 h and passivated under a flow of 5% O_2/He (30 mL/min) for 15 min at room temperature. After reduction and passivation, the catalysts were placed in the IV cell and were reduced under a flow of H_2 (30 mL/min) at 400 °C for 1 h.

Thermogravimetric analyses (TGA) were carried out in Setaram LabSys with a heating rate of 10 °C/min, under synthetic airflow of 25 mL/min in the 25–1000 °C *T*-range.

Reaction conditions

Ethanol SR was carried out in a fixed bed reactor with 12 mm of inner diameter, at atmospheric pressure. The catalysts were evaluated at 400, 500 and 600 °C. Before the reactions, the samples (20 mg) were reduced with pure H_2 (50 mL/min) at 800 °C for 1 h and then purged with N_2 during 15 min. The mixture of reagents was obtained using two saturators containing ethanol and water, separately, and streams of N_2 (30 mL/min) passing through each of them. The saturators were kept at the necessary temperature to obtain the desired H_2O/ethanol molar ratio of 3.0 (2.5 mol% ethanol; 7.5 mol% H_2O, 90.0 mol% N_2).

The mixture of reagents (H_2O/ethanol) and the reaction products were analyzed by a GC Agilent

7890A Gas Chromatograph, equipped with two detectors (thermal conductivity detector (TCD) and flame ionization detector (FID)) and two columns (molecular sieve and PLOT U). Ethanol conversion ($X_{ethanol}$) (Eq. 1) and product distribution (S_x) (Eq. 2) were determined as follows:

$$X_{ethanol} = \frac{(n_{ethanol})fed - (n_{ethanol})exit}{n_{ethanol}} \times 100 \quad (1)$$

$$S_x = \frac{(n_x)produced}{(n_{total})produced} \times 100 \quad (2)$$

where (n_x) produced = moles of x produced (x = reaction products) and (n_{total}) produced = sum of the moles of products produced (the water moles produced are not included).

Results and discussion

Catalyst characterization

The specific BET area and chemical composition of the catalysts and SiO_2 support are shown in Table 1. The SiO_2 nanospheres presented a low surface area of 32.9 m^2/g increased by the insertion of Ni (89.1 m^2/g). The addition of CeO_2 at the Ni–SiO_2 catalysts also increased the surface area of the material to 101.8 m^2/g. The N_2 adsorption/desorption isotherms and pore size distribution for Ni–CS, Ni–SiO_2 and SiO_2 are shown in Fig. 2. Their adsorption isotherms are apparently classified as the types IV, representing multilayer adsorption and capillary condensation in mesoporous materials even though contribution of micropore filling to the isotherms could not be judged. The average pore size of the SiO_2 was 35.9 nm and it decreased with the insertion of Ni and CeO_2 in the support. The average pore size was 13.2 nm and 8.9 nm for the Ni–SiO_2 catalyst and the Ni–CS catalyst, respectively. Although the average pore sizes decreased considerably, the pore sizes remained in the range of 2 to 50 nm, characterizing these materials as mesoporous materials. This result suggests that the CeO_2 shell layer of the Ni–CS catalyst should not present significant resistance to the mobility of the reactants by the catalyst structure. The amount of Ni presented in Ni–CS catalyst was close to the expected 10%. On the other hand, the Ni content was a little higher than expected for the Ni/CeO_2 catalyst.

The materials were characterized by X-ray powder diffraction (Fig. 3) to determine the crystalline structure obtained. The Ni–SiO_2 catalyst shows a large XRD peak at 20–30° corresponding to the amorphous SiO_2 phase (JCPDS 82-1579) and weak diffraction peaks characteristic of Ni-phyllosilicate phase at 34.8, 37 and 61.7° (JCPDS 49-1859). The Ni/CeO_2 catalyst shows diffraction peaks characteristic of fluorite CeO_2, cubic face centered structure with diffraction peaks corresponding to planes (111), (200), (220), (311) (JCPDS 34-394). Relatively low intensity diffraction lines corresponding to NiO (JCPDS 44-1159) can also be observed.

The Ni–CS catalyst has diffraction peaks characteristic of the fluorite phase of CeO_2 and a weak and broad peak corresponding to the NiO and Ni-phyllosilicate phases. The crystallite sizes determined with the Scherrer equation for CeO_2 in Ni–CS and Ni/CeO_2 catalysts were 5.3 and 33.4, respectively.

Temperature-programmed reduction (TPR) analyzes were recorded for Ni–SiO_2 and Ni–CS catalysts (Fig. 4) in order to evaluate the Ni–SiO_2 interaction, as well as the effect of CeO_2 shell on catalyst reducibility. The TPR profile of Ni–SiO_2 catalyst showed two main reduction ranges. The H_2 consumption at low temperature around 375–445 °C may be related to the reduction of Ni^{2+} to Ni^0 due to weak interactions between the nickel oxide and the silica support. In contrast, the reduction range of

Table 1 Specific BET area, pore size, pore volume and chemical composition of the catalyst and SiO_2 support

Sample	BET surface area (m^2/g)	Pore size (nm)	Pore volume (cm^3/g)	Chemical composition (%)		
				Ni	SiO_2	CeO_2
Ni–CS	101.8	8.9	0.23	11.4	18.6	70.0
Ni–SiO_2	89.1	13.2	0.29	13.1	86.9	–
SiO_2	32.9	35.9	0.30	–	–	–
Ni/CeO_2	–	–	–	15.2	–	84.8

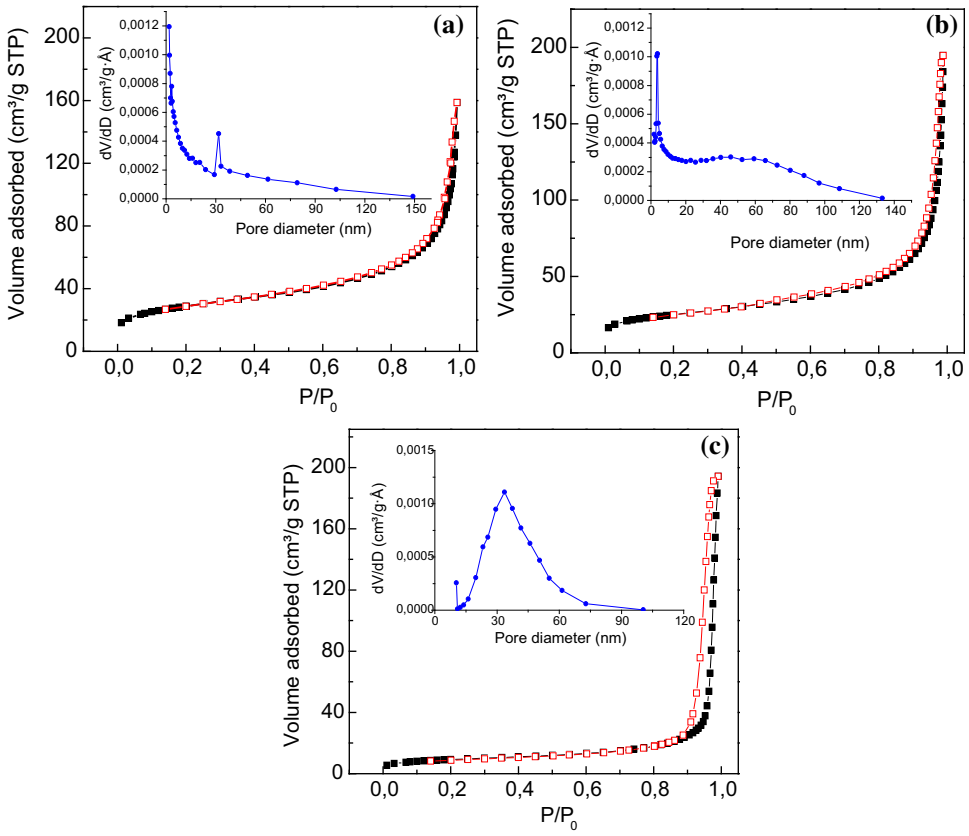

Figure 2 N_2 adsorption/desorption isotherms and pore size distribution for **a** Ni–CS, **b** Ni–SiO_2 and **c** SiO_2.

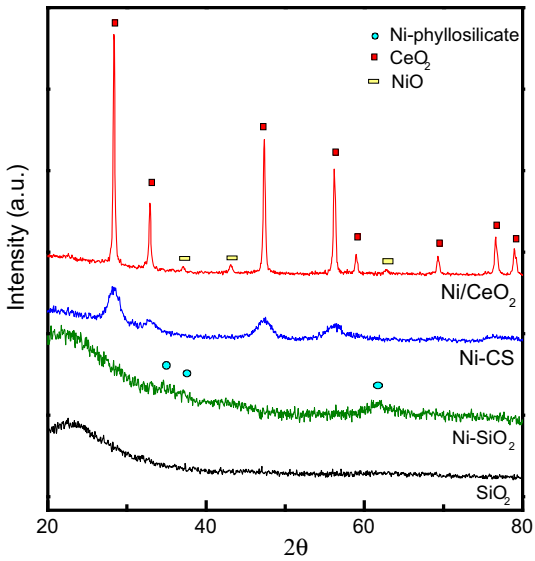

Figure 3 XRD patterns of SiO_2 support and catalysts.

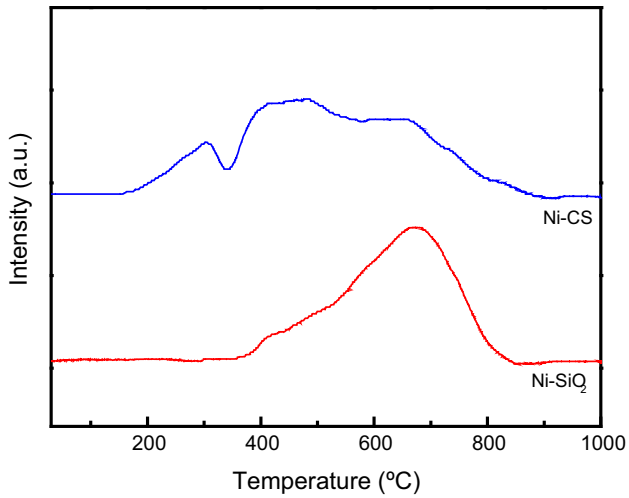

Figure 4 Ni–SiO_2 and Ni–CS catalysts H_2-TPR profiles.

about 675 °C may be related to Ni^{2+} in the phyllosilicate structure reduction as it has a stronger interaction with silica making it more difficult to reduce [18].

Ni–CS catalyst TPR profile shows three main reduction ranges. The first one around 200–350 °C can be related to the reduction of oxygen species found in Ce_xNi_yO vacancies, promoted by entrance of Ni^{2+} cations into CeO_2 lattice replacing some Ce^{4+} ions [22]. The second range of hydrogen consumption around 350–550 °C can be associated to the

reductions of NiO to Ni^0 and Ce^{4+} to Ce^{3+}. Finally, the broad range peak at high temperature (550–850 °C) can be related to the reduction of the nickel with strong interaction with SiO_2 support [18].

The morphologies of the freshly prepared Ni–SiO_2 catalyst and the calcined SiO_2 support, Ni–SiO_2 and Ni–CS catalysts were analyzed by TEM (Fig. 5a–d). The TEM image obtained for SiO_2 support (Fig. 5a) show spherical shaped silica nanoparticles of ~100 nm, obtained by the Stöber method. Freshly prepared Ni–SiO_2 catalyst TEM image show that Ni-phyllosilicate formed over the silica spheres (Fig. 5b) and after calcination nickel nanoparticles (2–10 nm) are deposited evenly on the silica support (Fig. 5c). In the TEM image of the Ni–CS catalyst after calcination, a layer of CeO_2 coating the silica spheres can be observed (Fig. 5d). TEM-EDS mapping (Fig. 6) for Ni-CS catalyst show that Si is concentrated inside the spheres, while Ni are uniformly distributed on Si core and the relative intensity of the CeO_2 suggests the formation of a thin shell over the SiO_2.

In-situ DRIFTS analysis

The Ni–CS catalyst was first evaluated by an in situ analysis by diffuse reflectance infrared Fourier transform spectroscopy (DRIFTS) in the ESR at low temperatures. The analyzes were carried out from 30 to 400 °C in order to evaluate the possible paths of the steam reforming reaction in this catalyst in this temperature range. In situ DRIFT spectra obtained after exposure of the Ni–CS catalyst to a mixture of 0.5% ethanol and 1.5% water (equilibrium with He) at 30 °C for 30 min and subsequent gradual heating to 400 °C, under continuous flow of the reaction mixture, are shown in Fig. 7.

It is observed that the spectrum recorded at 30 °C is dominated by bands corresponding to different vibrational modes of ethoxy species formed by dissociative adsorption of ethanol on Ce cations (2974, 2884 and 1373/cm) [23]. The band located at 1643/cm is probably related to the vibrational mode (C–O) of any adsorbed acetyl or acetaldehyde species. These species can be produced by dehydrogenating a

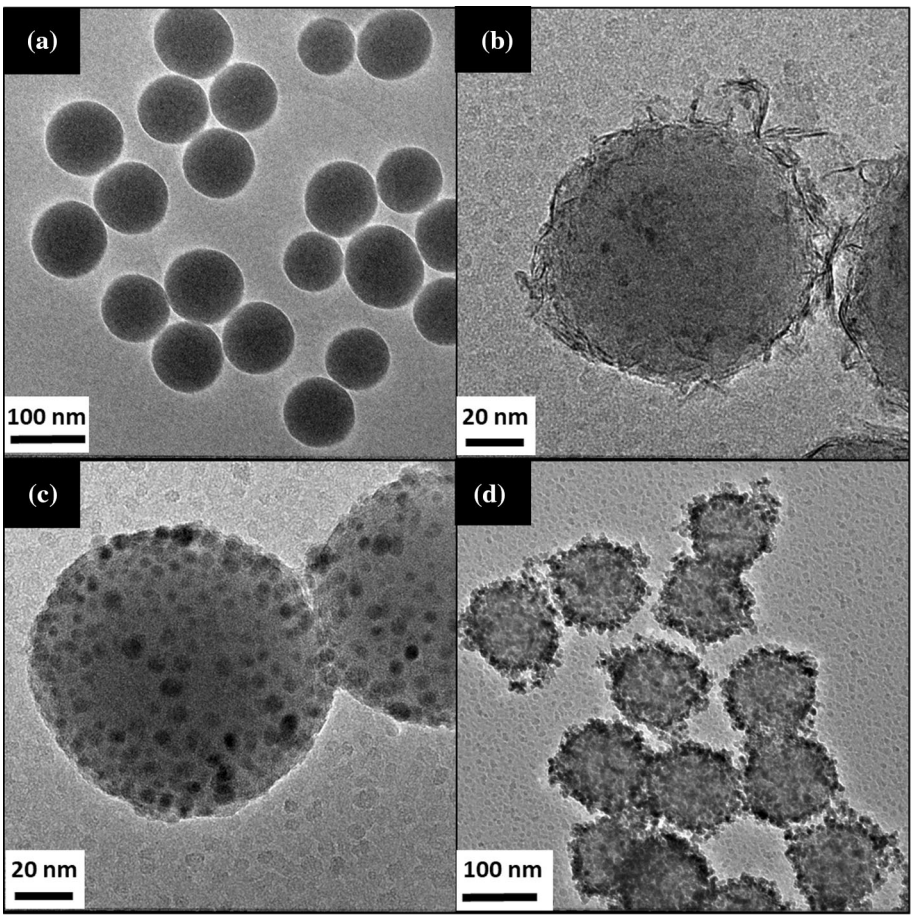

Figure 5 TEM images of **a** calcined silica support, **b** freshly prepared Ni–SiO_2 catalyst, **c** calcined Ni–SiO_2 catalyst, and **d** calcined Ni–CS catalyst.

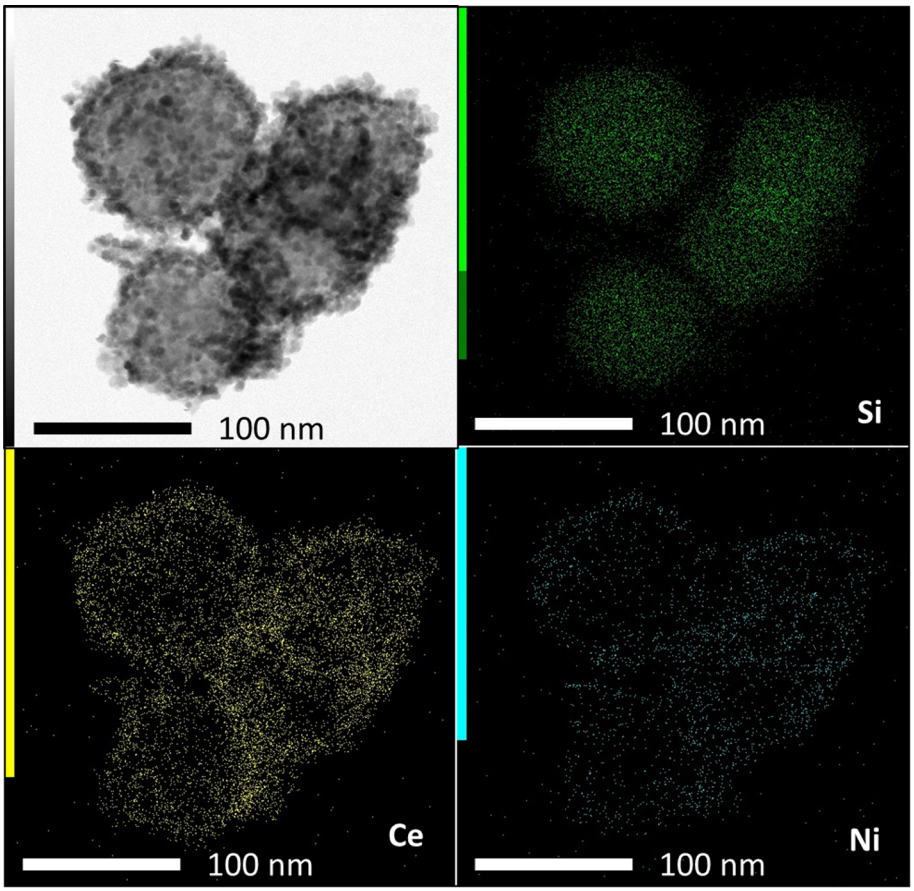

Figure 6 TEM-EDS mapping for Ni–CS catalyst.

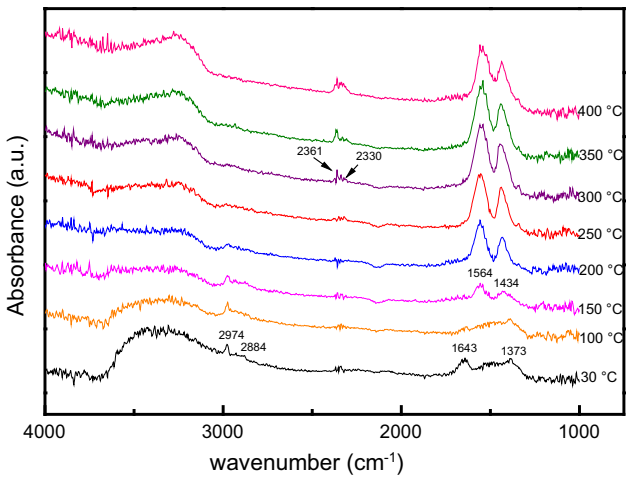

Figure 7 In situ DRIFT spectra of the Ni–CS catalyst at ESR from 30 to 400 °C.

fraction of the ethoxy species to acetaldehyde, which can be dehydrogenated to acetyl species [23]. Heating up to 100 °C causes virtually no changes in the ethoxy bands; however, there is a decrease in the band related to adsorbed acetyl or acetaldehyde species. After heating to 150 °C, the intensity of the ethoxy bands decreases significantly, with the appearance of new bands at 1434 and 1564/cm which, according to the literature [24], correspond to the modes of vibration (OCO) of acetate species. According to Lima et al. [25], the decomposition of ethoxy species can occur in two ways: decomposition to CO, CH_4 and H_2 or dehydrogenation to form acetaldehyde and acetyl species. Dehydrogenated species can form acetate through oxidation, with the participation of CeO_2 using the oxygen sites available on its surface. The condensation of two acetate molecules can lead to the formation of acetone favoring the formation of coke on the catalyst surface. At 300 °C, there is formation of CO_2 in the gaseous phase (2330 and 2361/cm) and as temperature increases its concentration increases.

ESR

First, the Ni–CS catalyst was evaluated in the ESR at 400 °C (Fig. 8). The catalyst showed high deactivation and selectivity to acetaldehyde. As seen by the

in situ analysis carried out by DRIFTS, the ethanol reforming route in this catalyst is through the dehydrogenation of ethanol to acetaldehyde followed by acetate species formation. Up to a temperature of 400 °C the reform of acetaldehyde to other products cannot be observed. Probably the acetate species are forming acetone, which is leading to coke formation on the catalyst surface causing deactivation. Therefore, it was necessary to increase the reaction temperature in order to avoid the acetate molecules condensation. So, the Ni–CS, Ni–SiO_2 and Ni/CeO_2 catalysts were evaluated at the temperatures of 500 and 600 °C.

Figure 9 presents the conversion of ethanol and distribution of the products as a function of time on stream (TOS) for ESR at 500 °C, over Ni–SiO_2, Ni/CeO_2, and Ni–CS catalysts. All catalysts showed initial ethanol conversion of 100% constant during 20 h of reaction. H_2 selectivity was around 70% for Ni/CeO_2 and Ni–CS catalysts and a little lower for Ni–SiO_2 catalyst. Ni catalysts are very active for C–C bond scission and according to the previously proposed ethanol conversion reactions mechanism [26], ethanol can be easily decomposed to H_2, CH_4 and CO (Eq. 3) or it is firstly dehydrogenated to acetaldehyde and H_2 (Eq. 4). Acetaldehyde can be decomposed to CH_4 and CO (Eq. 5) or desorb in the gas phase. Subsequently, CH_4 steam reforming (Eq. 6) and water gas shift (WGS) reaction (Eq. 7) proceed to produce H_2 and CO_2.

$$C_2H_5OH \rightarrow H_2 + CH_4 + CO \quad (3)$$

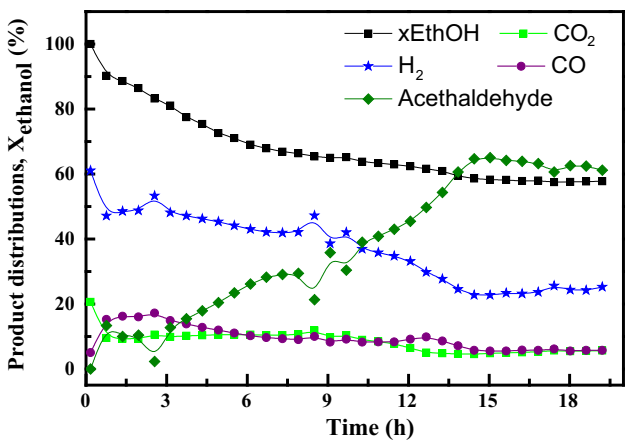

Figure 8 Ethanol conversion and product distributions for ESR at 400 °C over Ni–CS catalysts.

$$C_2H_5OH \rightarrow C_2H_4O + H_2 \quad (4)$$

$$C_2H_4O \rightarrow CH_4 + CO \quad (5)$$

$$CH_4 + H_2O \rightarrow CO + 3H_2 \quad (6)$$

$$CO + H_2O \rightarrow CO_2 + H_2 \quad (7)$$

H_2 and CO_2 with small amounts of CO and CH_4 were the main products detected for all catalysts at 500 °C, leading to believe that ethanol decomposition, or ethanol dehydrogenation with subsequent acetaldehyde decomposition, followed by CH_4 steam reforming (SR) and water gas shift (WGS) reaction may be the main reactions taking place.

The catalysts were also tested in ESR at 600 °C (Fig. 10). Since the water gas shift reaction is unfavorable at high temperatures, the increase in the temperature reaction decreases CO_2 formation and increases CO formation. The decrease in CH_4 formation can be explained by the fact that CH_4 SR reaction is favorable at high temperature.

The thermogravimetric analysis (Fig. 11) was carried out to investigate the carbon decomposition process of the post reaction samples. Ni/CeO_2 catalyst after the reaction at 500 °C showed 2 peaks of weight loss at 500 and 626 °C that indicates different types of carbonaceous species formed on the catalyst surface. Increasing the reaction temperature, Ni/CeO_2 catalyst TG profile showed only one peak at a higher temperature (638 °C). According to the literature [27], the oxidation of amorphous carbonaceous species take place at low temperature and graphitic carbon is oxidized at high temperature. Therefore, the weight loss at 500 °C can be assigned to oxidation of amorphous carbonaceous species while the peaks at 626 °C and 638 °C are related to the oxidation of graphitic carbon. TG profiles of Ni–SiO_2 and Ni–CS catalysts after reactions at 500 °C showed only one peak at 580 °C and 536 °C, respectively. The TG profile of the Ni–SiO_2 catalyst after high-temperature reaction (600 °C) showed only one peak (595 °C).

The amount of carbon formed during the reaction for the different catalysts and temperature reactions is listed in Table 2. Ni–SiO_2 catalyst reaction at 500 °C showed the highest carbon formation (18.3 mgC/(gcat.h)) compared to the other catalysts. On the other hand, for the Ni–CS catalyst the amount of carbon formed was only 3.7 mgC/(gcat.h) during the reaction at 500 °C. This can be explained by the presence of the CeO_2 structure in the Ni/CeO_2 and Ni–CS

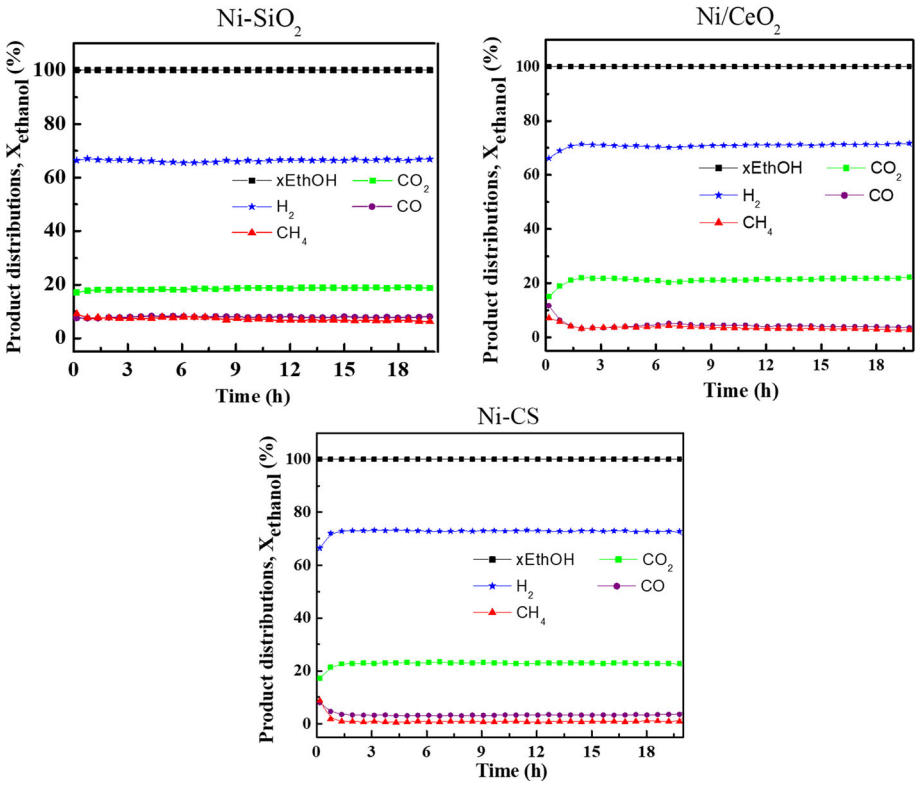

Figure 9 Ethanol conversion and product distributions for ESR at 500 °C over Ni–SiO_2, Ni/CeO_2, and Ni–CS catalysts.

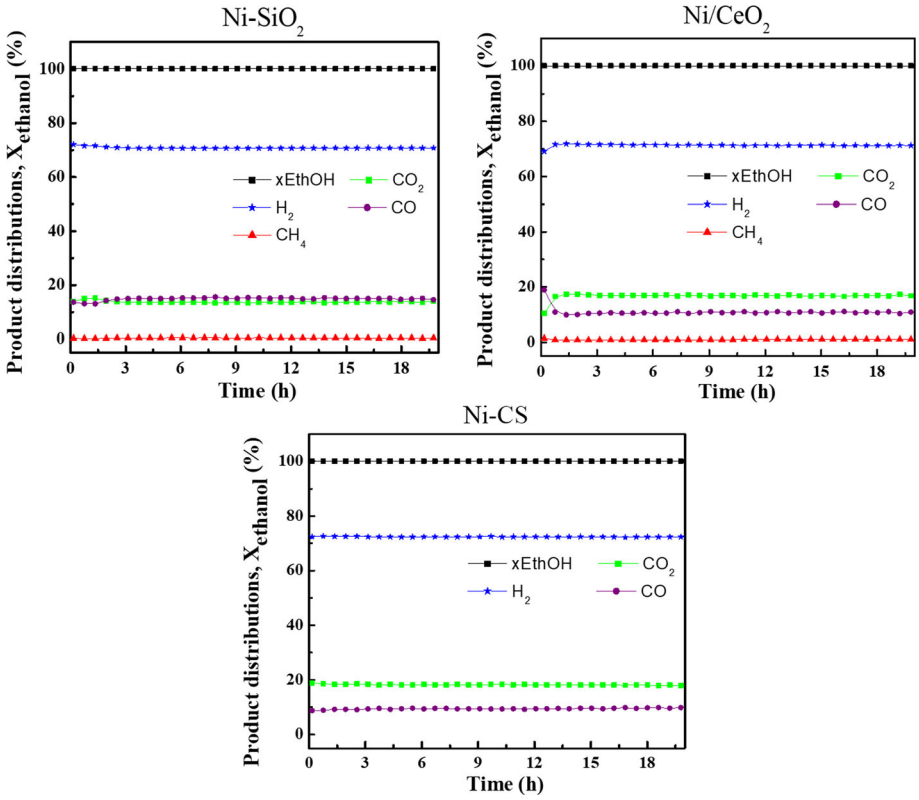

Figure 10 Ethanol conversion and product distributions for ESR at 600 °C over Ni–SiO_2, Ni/CeO_2, and Ni–CS catalysts.

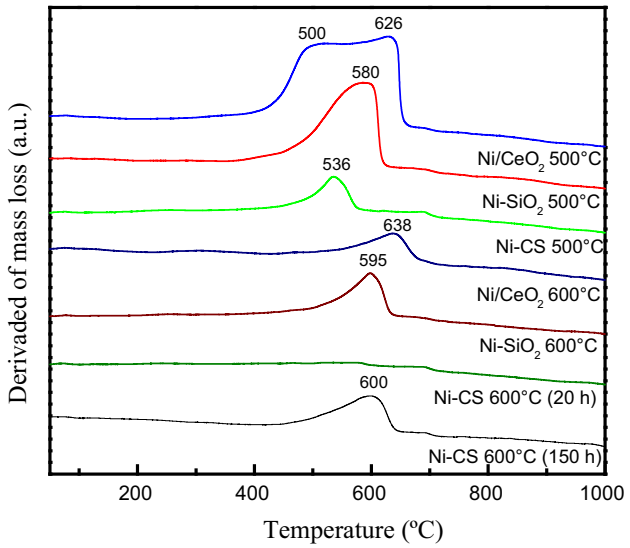

Figure 11 TG derivative of spent catalysts Ni/CeO_2, Ni–SiO_2, Ni–CS after 20 h of ESR at 500 and 600 °C and Ni–CS after 150 h of ESR at 600 °C.

Table 2 Amount of carbon formed for the different catalysts after ethanol SR reactions at 500 and 600 °C

Sample	Temperature reaction (°C)	mgC/(gcat.h)
Ni–SiO_2	500	18.3
Ni/CeO_2	500	17.7
Ni–CS	500	3.7
Ni–SiO_2	600	6.3
Ni/CeO_2	600	5.2
Ni–CS	600	–

catalysts. The oxygen exchange capacity of CeO_2 in the catalyst surface can help to remove carbon formed throughout the reaction.

The increase in the reaction temperature led to a decrease in carbon formation on the surface of the Ni/CeO_2 and Ni–SiO_2 catalysts, which can be explained by the favoring of the Boudouard reaction (Eq. 8) with the increase in the reaction temperature.

$$CO_2 + C \rightleftharpoons 2CO \quad (8)$$

In the case of the Ni–CS catalyst, the presence of carbon deposit on the catalyst surface was not observed during 20 h of reaction at 600 °C under the conditions used in the experiment.

In order to evaluate the performance of the Ni–CS catalyst in stationary applications for long periods of continuous H_2 supply, the catalyst was tested in a long durability reaction (Fig. 12). The catalyst

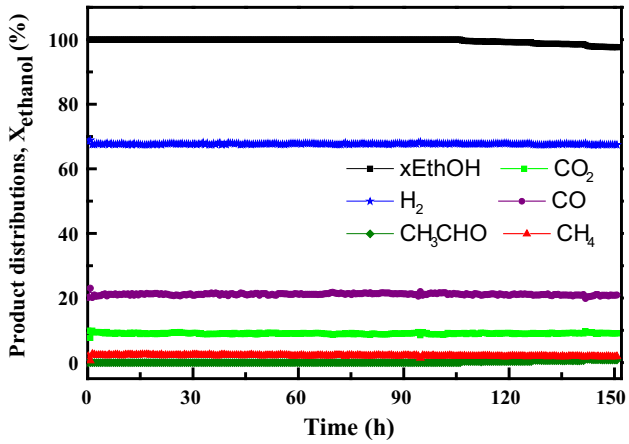

Figure 12 Ethanol conversion and product distributions for long time ESR at 600 °C over Ni–CS catalysts.

showed high activity with low deactivation after 100 h of reaction. The presence of carbon deposited on the catalyst surface after reaction was evaluated by thermogravimetric analysis (Fig. 11). The TG profiles of Ni–CS catalyst after reaction at 600 °C for 150 h showed only one peak at 600 °C and a very low carbon formation amount of 1.3 mgC/(gcat.h).

Conclusions

Spherical shaped silica nanoparticles of ~100 nm were obtained by Stöber method. TEM image of catalysts showed nickel nanoparticles (2–10 nm) well dispersed on the silica support and a layer of CeO_2 coating the silica spheres.

All catalysts tested showed high activity with 100% conversion of ethanol and remained constant during all reactions. However, in terms of coke inhibition, the Ni–CS catalyst presents a superior performance compared to catalysts without CeO_2 shell. The effect of the catalyst structured in a core–shell shape, with cerium oxide covering the Ni particles, gave the catalyst greater capacity to remove the carbon formed during the ESR reactions. Ni–CS catalyst showed excellent stability and coke inhibition properties for at least 100 h on ESR reaction at 600 °C.

Acknowledgements

The authors thank IPEN-CNEN/SP for supporting this research and FAPESP (2019/115110-2) for the scholarship support.

References

[1] Mckendry P (2002) Energy production from biomass (part 1): overview of biomass. Bioresour Technol 83:37–46

[2] Holladay JD, Hu J, King DL, Wang Y (2009) An overview of hydrogen production technologies. Catal Today 139:244–260

[3] Busca G, Costantino U, Montanari T, Ramis G, Resini C, Sisani M (2010) Nickel versus cobalt catalysts for hydrogen production by ethanol steam reforming: Ni–Co–Zn–Al catalysts from hydrotalcite-like precursors. Int J Hydrog Energy 35:5356–5366

[4] Vicente J, Erena J, Olazar M, Benito PL, Bilbao J, Gayubo AG (2014) Kinetic behaviour of commercial catalysts for methane reforming in ethanol steam reforming process. J Energy Chem 23:639–644

[5] Li M, Li S, Zhang C, Wang S, Ma X, Gong J (2011) Ethanol steam reforming over Ni/NixMg1–xO: inhibition of surface nickel species diffusion into the bulk. Int J Hydrog Energy 36:326–332

[6] Alberton AL, Souza MMVM, Schmal M (2007) Carbon formation and its influence on ethanol steam reforming over Ni/Al_2O_3 catalysts. Catal Today 123:257–264

[7] da Silva ALM, den Breejen JP, Mattos LV, Bitter JH, de Jon KP, Noronha FB (2014) Cobalt particle size effects on catalytic performance for ethanol steam reforming–Smaller is better. J Catal 318:67–74

[8] Wang H, Liu Y, Wang L, Qin YN (2008) Study on the carbon deposition in steam reforming of ethanol over Co/CeO_2 catalyst. Chem Eng J 145:25–31

[9] Garbarino G, Lagazzo A, Riani P, Busca G (2013) Steam reforming of ethanol–phenol mixture on Ni/Al_2O_3: effect of Ni loading and sulphur deactivation. Appl Catal B 129:460–472

[10] Rocchini E, Trovarelli A, Llorca J, Graham GW, Weber WH, Maciejewski M, Baiker A (2000) Relationships between structural/morphological modifications and oxygen storage–redox behavior of silica-doped ceria. J Catal 194:461–478

[11] Dutta P, Pal S, Seehra MS, Shi Y, Eyring EM, Ernst RD (2006) Concentration of Ce^{3+} and oxygen vacancies in cerium oxide nanoparticles. Chem Mater 18(21):5144–5146

[12] Yang SC, Su WN, Rick J, Lin SD, Liu JY, Pan CJ, Lee JF, Hwang BJ (2013) Oxygen vacancy engineering of cerium oxides for carbon dioxide capture and reduction. Chemsuschem 6(8):1326–1329

[13] Ciambell P, Palma V, Ruggiero A, Iaquaniello G (2009) Platinum catalysts for the low temperature catalytic steam reforming of ethanol. Chem Eng Trans 17:19–24

[14] Costa LOO, Vasconcelos SMR, Pinto AL, Silva AM, Mattos LV, Noronha FB, Borges LEP (2008) Rh/CeO_2 catalyst preparation and characterization for hydrogen production from ethanol partial oxidation. J Mater Sci 43:440–449. https://doi.org/10.1007/s10853-007-1982-2

[15] Moraes TS, Rabelo Neto RC, Ribeiro MC, Mattos LV, Kourtelesis M, Ladas S, Verykios X, Noronha FB (2016) Ethanol conversion at low temperature over CeO_2—supported Ni-based catalysts. Effect of Pt addition to Ni catalyst. Appl Catal B 181:754–768

[16] Mattos LV, Jacobs G, Davis BH, Noronha FB (2012) Production of hydrogen from ethanol: review of reactions mechanism and catalyst deactivation. Chem Rev 112:4094–4123

[17] Kawi S, Kathiraser Y, Ni J, Oemar U, Li Z, Saw ET (2015) Progress in synthesis of highly active and stable nickel-based catalysts for carbon dioxide reforming of methane. Chemsuschem 21:3556–3575

[18] Das S, Ashok J, Bian Z, Dewangan N, Wai MH, Du Y, Borgna A, Hidajat K, Kawi K (2018) Silica–ceria sandwiched Ni core–shell catalyst for low temperature dry reforming of biogas: coke resistance and mechanistic insights. Appl Catal B 230:220–236

[19] Stöber W, Fink A (1968) Controlled growth of monodisperse silica spheres in the micron size range. J Colloid Interface Sci 26:62–69

[20] Zhang T, Zhang Q, Ge J, Goebl J, Sun M, Yan Y, Liu Y, Chang C, Guo J, Yin Y (2009) A self-templated route to hollow silica microspheres. J Phys Chem C 113(8):3168–3175

[21] Ding S, Hu X, Guan P, Zhang N, Li J, Gao X, Zhang X, Ding X, Du C (2017) Preparation of surface-imprinted microspheres using ionic liquids as novel cross-linker for recognizing an immunostimulating peptide. J Mater Sci 52:8027–8040. https://doi.org/10.1007/s10853-017-1005-x

[22] Strandwitz NC, Stucky GD (2009) Hollow microporous cerium oxide spheres template by colloidal silica. Chem Mater 21:4577–4582

[23] Mattos LV, Jacobs G, Davis BH, Noronha FB (2012) Production of hydrogen from ethanol: review of reaction mechanism and catalyst deactivation. Chem Rev 112:4094–4123

[24] Silva AM, Farias AMD, Costa LOO, Barandas APMG, Mattos LV, Fraga MA, Noronha FB (2008) Partial oxidation and water-gas shift reaction in an integrated system for hydrogen production from ethanol. Appl Catal A 34:179–186

[25] Lima SM, Da Cruz IO, Jacobs G, Davis BH, Mattos LV, Noronha FB (2008) Steam reforming, partial oxidation, and oxidative steam reforming of ethanol over Pt/$CeZrO_2$ catalyst. J Catal 257:356–368

[26] Ogo S, Sekine Y (2020) Recent progress in ethanol steam reforming using non-noble transition metal catalysts: a review. Fuel Process Technol 199:106238–106249

[27] Koo KY, Roh H, Seo YT, Dong JS, Wang LY, Seung BP (2008) Coke study on MgO-promoted Ni/Al_2O_3 catalyst in combined H_2O and CO_2 reforming of methane for gas to liquid (GTL) process. Appl Catal A 340:183–190